batteries

MDPI

Article

Novel One-Step Production of Carbon-Coated Sn Nanoparticles for High-Capacity Anodes in Lithium-Ion Batteries

Emma M. H. White [1,*], Lisa M. Rueschhoff [2], Steve W. Martin [3] and Iver E. Anderson [3,4]

[1] Materials and Corrosion Division, DECHEMA Research Institute, Theodor-Heuss-Allee 25, 60486 Frankfurt am Main, Germany
[2] Air Force Research Laboratory, Materials and Manufacturing Directorate, Wright-Patterson Air Force Base, Dayton, OH 45433, USA; lisa.rueschhoff.1@us.af.mil
[3] Department of Materials Science and Engineering, Iowa State University, 2220 Hoover Hall, Ames, IA 50011, USA; swmartin@iastate.edu (S.W.M.); andersoi@iastate.edu (I.E.A.)
[4] The United States Department of Energy's Ames National Laboratory, 222 Metals Development, Ames, IA 50011, USA; andersoi@ameslab.gov
* Correspondence: emma.white@dechema.de

Abstract: Lithium-ion batteries offer the highest energy density of any currently available portable energy storage technology. By using different anode materials, these batteries could have an even greater energy density. One material, tin, has a theoretical lithium capacity (994 mAh/g) over three-times higher than commercial carbon anode materials. Unfortunately, to achieve this high capacity, bulk tin undergoes a large volume expansion, and the material pulverizes during cycling, giving a rapid capacity fade. To mitigate this issue, tin must be scaled down to the nano-level to take advantage of unique micromechanics at the nanoscale. Synthesis techniques for Sn nanoparticle anodes are costly and overly complicated for commercial production. A novel one-step process for producing carbon-coated Sn nanoparticles via spark plasma erosion (SPE) shows great promise as a simple, inexpensive production method. The SPE method, characterization of the resulting particles, and their high-capacity reversible electrochemical performance as anodes are described. With only a 10% addition of these novel SPE carbon-coated Sn particles, one anode composition demonstrated a reversible capacity of ~460 mAh/g, achieving the theoretical capacity of that particular electrode formulation. These SPE carbon-coated Sn nanoparticles are drop-in ready for present commercial lithium-ion anode processing and would provide a ~10% increase in the total capacity of current commercial lithium-ion cells.

Keywords: tin; carbon; nanoparticles; Li-ion battery anode; spark plasma erosion

Citation: White, E.M.H.; Rueschhoff, L.M.; Martin, S.W.; Anderson, I.E. Novel One-Step Production of Carbon-Coated Sn Nanoparticles for High-Capacity Anodes in Lithium-Ion Batteries. *Batteries* **2024**, *10*, 386. https://doi.org/10.3390/batteries10110386

Academic Editors: Wenquan Lu, Likun Zhu and Yuzi Liu

Received: 16 September 2024
Revised: 28 October 2024
Accepted: 29 October 2024
Published: 1 November 2024

1. Introduction

The widespread uses of portable electronics and massive efforts to extend the range of electric vehicles have greatly motivated the search for higher energy density portable power sources. Of the currently available energy storage technologies, lithium-ion batteries offer one of the highest energy densities, both volumetrically and gravimetrically [1]. Sony produced the first commercial Li-ion cells in the early 1990s with a lithium cobalt oxide cathode and a graphitic carbon anode [2]. While these cells have good safety and cyclability, their capacity is inherently limited due to the anode and cathode materials used. In particular, the anode has potential for increasing cell capacity since there are many materials with a higher theoretical capacity than the 372 mAh/g capacity of carbon. Of these alternatives, Sn has one of the highest known capacities at 990 mAh/g and high electronic conductivity, which is important for high-rate cells and would reduce the amount of carbon necessary for electrode conductivity [3].

Tin is not currently used as a Li-ion anode material because of its limited bulk cyclability. When Sn alloys with Li, the crystal structure volume expands drastically (~300%), which

can cause the material to disintegrate, leading to a rapid capacity fade during cycling [4]. Nanoscale Li reactive materials have been found to improve electrochemical performance through the following: (1) shorter diffusion distances increasing charge/discharge rates, (2) larger volume expansion allowed due to unique mechanical properties, and (3) structural changes from thermodynamic and kinetic properties [5]. Many investigations have been conducted on nanoscale composite anodes of Sn, such as nano-wires, nano-films, and nanoparticles, with resulting improvements in the capacity and cyclability of the materials. Xu and co-workers obtained notably high capacities at high rates by dispersing 10 nm Sn within a spherical carbon matrix [4]. Zhou et al. obtained 533.4 mAh/g at 100 mA/g current density after 50 cycles by fabricating Sn-based composite chrysanthemum-like microstructures of SnO_2 nanoparticles [6]. The capacity faded due to the expansion of particles and collapse of the structure, producing a fresh interface to react and form further solid electrolyte interphase (SEI) layers in addition to agglomeration of the particles that were produced at higher temperatures [6].

Though these materials reached higher capacities with good cyclability, in general, the methods to produce them are costly and complicated to scale up for the large-quantity production required for practical commercial applications. The production of well-dispersed Sn nanoparticles in a carbon matrix is challenging due to the low melting point of Sn and the tendency for aggregation during carbonization [7,8]. Thus, a simple one-step synthesis method with the potential for continuous production is highly desirable to produce nano-structured and nano-sized carbon-coated Sn nanoparticles for use in commercial lithium-ion batteries [9].

Micron-sized metallic powders [10,11], rapidly solidified metallic glass powders [12], and even rare-earth containing magnet alloy powders [13] have been produced through the process of spark plasma erosion (SPE). SPE is versatile and inexpensive, and the type of equipment required is widely commercialized as electric discharge machining (EDM), so it is extremely scalable and simple as a novel nanoparticle production method. This represents a substantial leap forward as most other methods are extremely complex, costly, or require multiple processing steps. In the plunge SPE process, two consumable, electrically conductive electrodes are separated by a small gap, submersed in a dielectric fluid, and connected to a pulsed external power source. When a sufficiently high electric field results from the applied voltage, breakdown of the dielectric fluid occurs, producing a spark discharge between the electrodes. Electrons emitted from the cathode and into the gap are energized from the electric field and ionize the molecules of the dielectric fluid. The resulting plasma channel (tens of microns in diameter, with temperatures >10,000 K and pressures ~300 MPa) transfers energy to locally heat the electrode surfaces [14]. This highly localized heating can eject vaporized and/or molten material from the electrode surfaces that is rapidly quenched by the dielectric fluid, forming particles [14]. The SPE-produced particles are generally bimodally distributed, likely due to these two modes (vapor or liquid) of ejection from the electrode surface [14].

To prevent oxidation and to obtain better electrochemical performance, it appears to be essential to coat the Sn nanoparticles with carbon, providing a forgiving matrix of passive particle surfaces [7,9]. Thus, the SPE process was explored using a conventional plunge EDM unit with Sn electrodes in a hydrocarbon dielectric (providing a carbon source for decomposition) as a novel one-step synthesis method to produce carbon-coated Sn nanoparticles on the order of ~20–200 nm [15].

2. Experimental Section

2.1. Spark Plasma Erosion (SPE)

Using kerosene (Sigma-Aldrich, St. Louis, MO, USA, reagent grade) as a dielectric fluid, 16 mm pure (99.99%) drop cast Sn rods (produced in-house) were SPE processed in a modified erosion chamber on a Sharp Industries, Inc. (Torrance, CA, USA) 300C series EDM. Table 1 lists the experimental parameters used in the SPE synthesis of the Sn particles. The particles were collected by centrifuging at 17,000 rpm for 20 min in a Beckman Coulter

(Indianapolis, IN, USA) Avanti-JE centrifuge with stainless-steel tubes in a JA-17 rotor. The solvent was exchanged from kerosene to hexane (Alfa-Aesar, Haverhill, MA, USA, n-Hexane HPLC grade 95+%) by using a sonic bath and 5 centrifuge runs, decanting the solvent and replacing with clean hexane after each run. The hexane-dispersed particles were dried under vacuum to obtain the particles for electrochemical testing.

Table 1. SPE key processing parameters.

Spark Time On	2 µs	Gap Voltage	1 V
Spark Time Off	4 µs	Polarity	Reverse
High-Voltage Current	0 A	Rotation Speed	~130 rpm
Low-Voltage Current	1.5 A		

2.2. Particle Characterization

A Tecnai G2 F20 transmission electron microscope (TEM) (FEI, Hillsboro, OR, USA) operating at 200 keV was used to obtain brightfield images, diffraction patterns and EDS of the SPE particles. X-ray photoelectron spectroscopy (XPS) of the particles was performed on a Perkin Elmer (Shelton, CT, USA) PHI 5500 ESCA system with a Ag filament.

2.3. Electrode Casting

Water-based slurries of SPE particles were made in 10:70:5:15, 20:60:5:15 and 80:0:5:15 weight ratios of SPE particles to graphite (Timrex, Paris, France, SFG 6L), to carbon black (Timrex, Super C65), to poly(acrylic acid) (PAA, Sigma-Aldrich, Mw ~450,000). Different ratios were used since Beattie et al. found that lowering the active material concentration of the electrodes, in this case Sn, achieved high capacity with good cyclability [16]. Additionally, the Sn nanoparticles have high enough conductivity that the graphite addition was eliminated in the 80:0:5:15 electrode. The SPE particles, carbons, and water were mixed using an ultrasonic probe for 1 min, followed by stirring in the PAA at 800 rpm for 1 h. The slurries were cast using a doctor blade set to ~250 µm on cleaned Cu foil (25 µm thick) and dried, and then 5/16-inch diameter disks were punched out of the castings for the electrodes.

2.4. Half-Cell Electrochemical Test Fixture

To minimize water contamination, and also to prevent reaction of the Li metal and the moisture-sensitive electrolyte, half-cells of the electrodes were constructed in an Ar atmosphere glovebox (<10 ppm O_2 and H_2O levels). A 2016 cover and can were used with the corresponding polypropylene gasket and nickel foam as the spacer and spring. Lithium metal (0.75 mm thick, Alfa Aesar, 99.9%) punched to 9/16-inch diameter was used as the counter-electrode. The separator was 25 µm thick Celgard (Charlotte, NC, USA) 2400 microporous polyethylene, punched to a 3/4-inch diameter circle. During assembly, 30 µL of 1 M $LiPF_6$ in ethylene carbonate/diethylene carbonate (1:1 ratio) electrolyte was added to the components to wet the separator and electrode.

2.5. Galvanostatic Charge/Discharge Cycling

The half-cells were electrochemically cycled using an ARBIN (College Station, TX, USA) BT-2000 system. Based upon their theoretical capacity (TC), the cells were cycled first at a TC/20 rate within a potential difference range of 0.01–1.0 V for 2 cycles with a taper charge to form the SEI layer and determine the actual capacity. The charge capacity from the second cycle was taken as the actual capacity (AC), and the cells were cycled from 0.01 to 1.0 V for 200 cycles at an AC/10 rate. To calculate the coulombic efficiency (%CE), the cycling data were analyzed according to Equation (1).

$$\%CE = 100\% - \left(\frac{discharge\ capacity - charge\ capacity}{discharge\ capacity} \right) \times 100\% \quad (1)$$

3. Results and Discussion

3.1. Particle Characterization

TEM brightfield images and a selected area diffraction pattern (SADP) of the SPE Sn particles are shown in Figure 1. Selected area diffraction of the general population evidenced diffuse rings, which matched well with the body-centered tetragonal phase of Sn (Table 2). The SPE Sn nanoparticles were bimodally distributed from ~20 nm to ~200 nm with smaller amorphous nanoparticles with some lattice fringes and larger crystalline particles based upon the TEM brightfield image contrast and the diffuse rings of the diffraction pattern. The size distribution and morphology align well with what has been previously reported [14,15,17]. XPS showed C1s, O1s and $Sn3d_{5/2}$ peaks in the measured spectra, as included in Figure 2. The O1s peak intensity decreased with etching and the $Sn3d_{5/2}$ peak shifted to lower binding energy. Thus, the SPE nanoparticles exhibited absorbed surface oxygen, likely due to sample exposure to the atmosphere just prior to insertion into the instrument, as well as an adhered, primarily aliphatic carbon surface layer [17–19]. This carbon surface layer character was exhaustively investigated and characterized in a previous publication focused on Sn-Si alloy SPE nanoparticles [17]. The TEM and XPS results are in accordance with the results from [17].

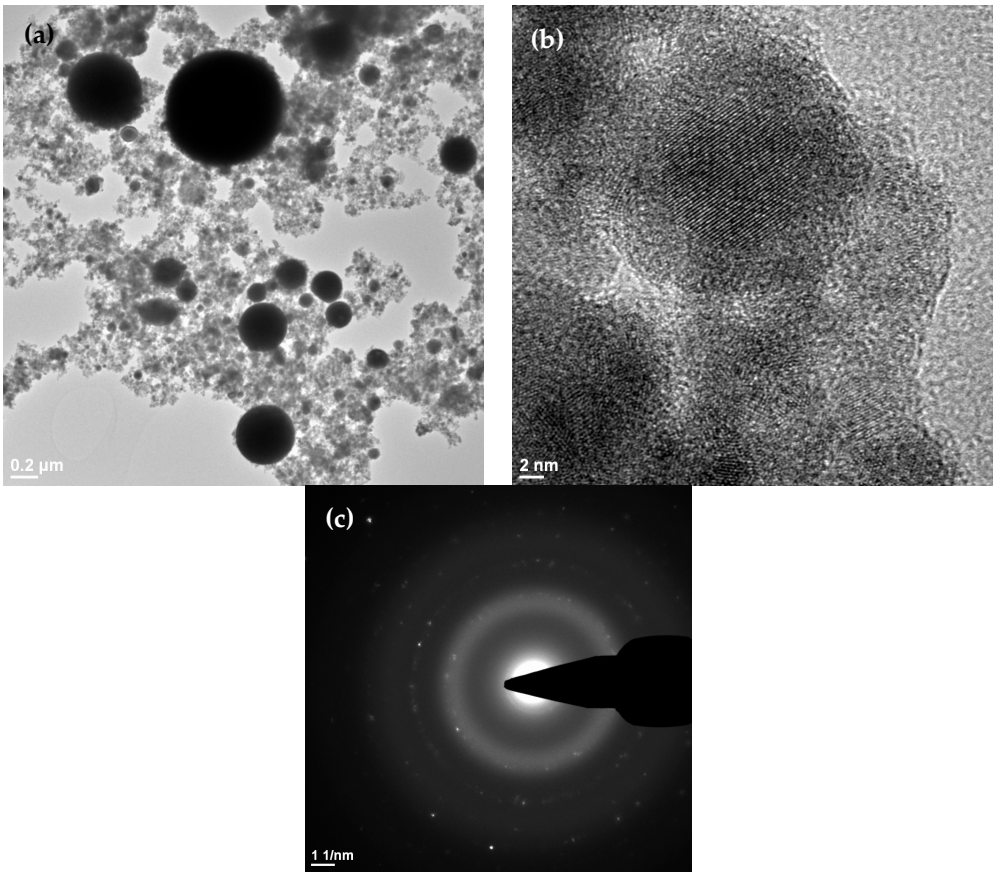

Figure 1. SPE Sn nanoparticle TEM images of general distribution (**a**) and high-resolution image (**b**) of smaller nanoparticles showing lattice fringes; (**c**) selected area diffraction pattern (SADP) of general distribution.

Table 2. SADP analysis of SPE Sn nanoparticles. Comparison of nearest-neighbor atom spacings from diffraction pattern rings (Figure 1c) and matching body-centered tetragonal Sn d-spacings.

hkl	Sn d (Å)	SADP avg. (This Work) d (Å)
011	2.79	2.73
220	2.06	1.98
031	1.66	1.60
240	1.30	1.38

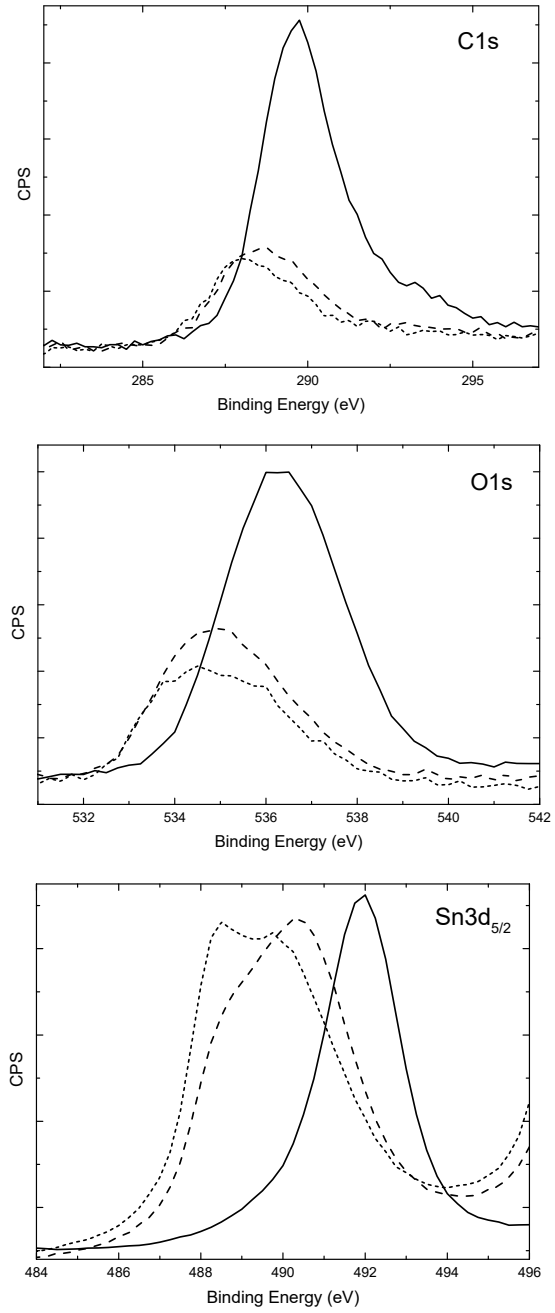

Figure 2. XPS spectra of SPE Sn nanoparticles: C1s peak, O1s peak and $Sn3d_{5/2}$ peak. Solid is pre-etching, long dashed is after Ar-ion etching ~5 min, and short dashed is after a further ~6 min etching. Approximate etching rate is 10 nm/minute. All data are shown without shifting from sample charging.

3.2. Electrochemical Performance

The ratios of SPE nanoparticles in the composite electrodes had a significant impact on the half-cell capacity. The 10:70:5:15 electrode had the highest capacity and greatest stability, as shown in Figure 3. For the 10:70:5:15 electrode, the initial capacity of the SPE Sn nanoparticles was greater than the theoretical (~450 mAh/g for the electrode), as shown in Figure 4. The initial irreversible capacity of 359 mAh/g is likely due to the formation of the SEI layer [7–9]. The cell then continued to cycle at ~460 mAh/g with a coulombic efficiency of >99.5% for over 200 cycles. The potential difference versus capacity shows full lithiation of the various phases of Sn [20], as labeled in Figure 5.

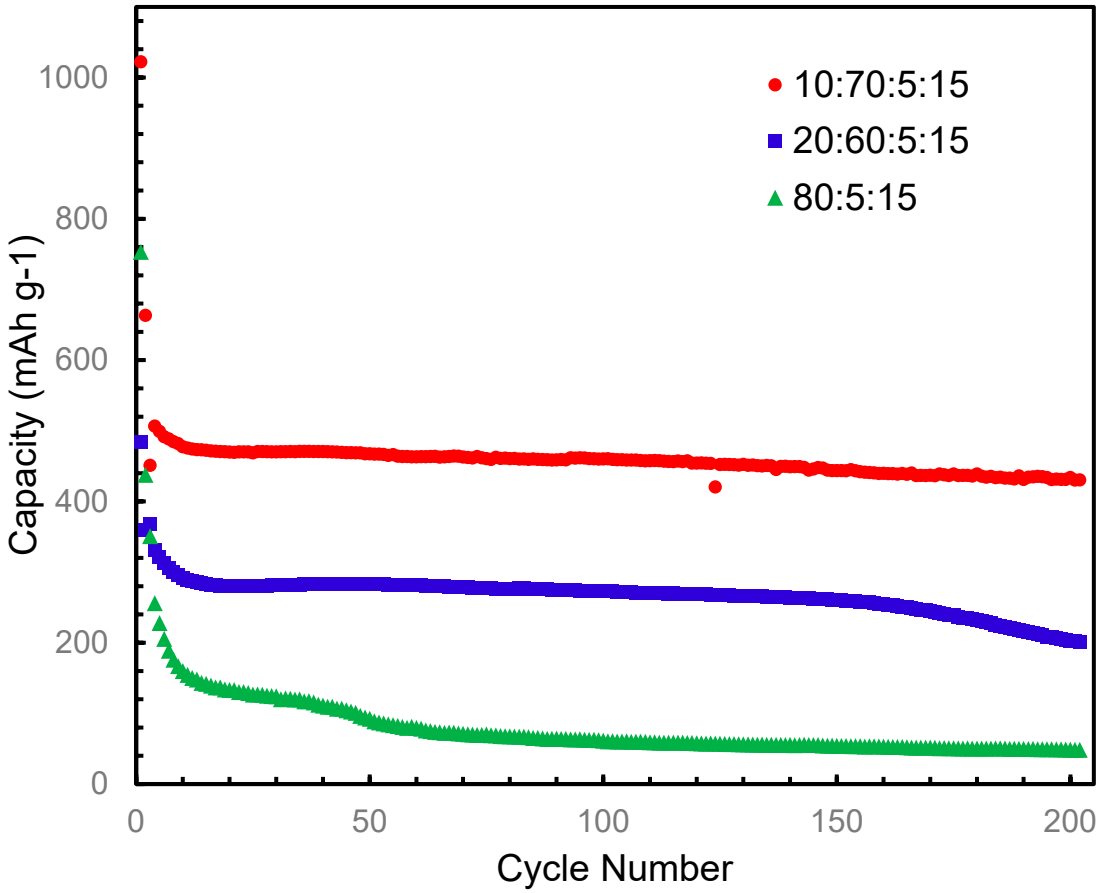

Figure 3. Capacity of SPE Sn nanoparticles for electrodes of varying active material ratios.

Electrodes with a higher amount of SPE Sn nanoparticles (ratios 20:60:5:15 and 80:5:15) had poorer stability and lower capacity, which is in agreement with Beattie et al. [16]. This is likely due to the poorer conductivity of the surface carbon layer, as it is comprised of primarily hydrocarbon species that are insulative to electrons and ions [17]. A larger concentration of particles means more of this less-conductive material limits the overall conductivity and, thus, capacity. Additionally, nanoparticles of Sn suffer aggregation issues during cycling, and a higher active material ratio will increase the proximity of Sn nanoparticles for possible aggregation, as well as reducing the available space for volume expansion [7,21].

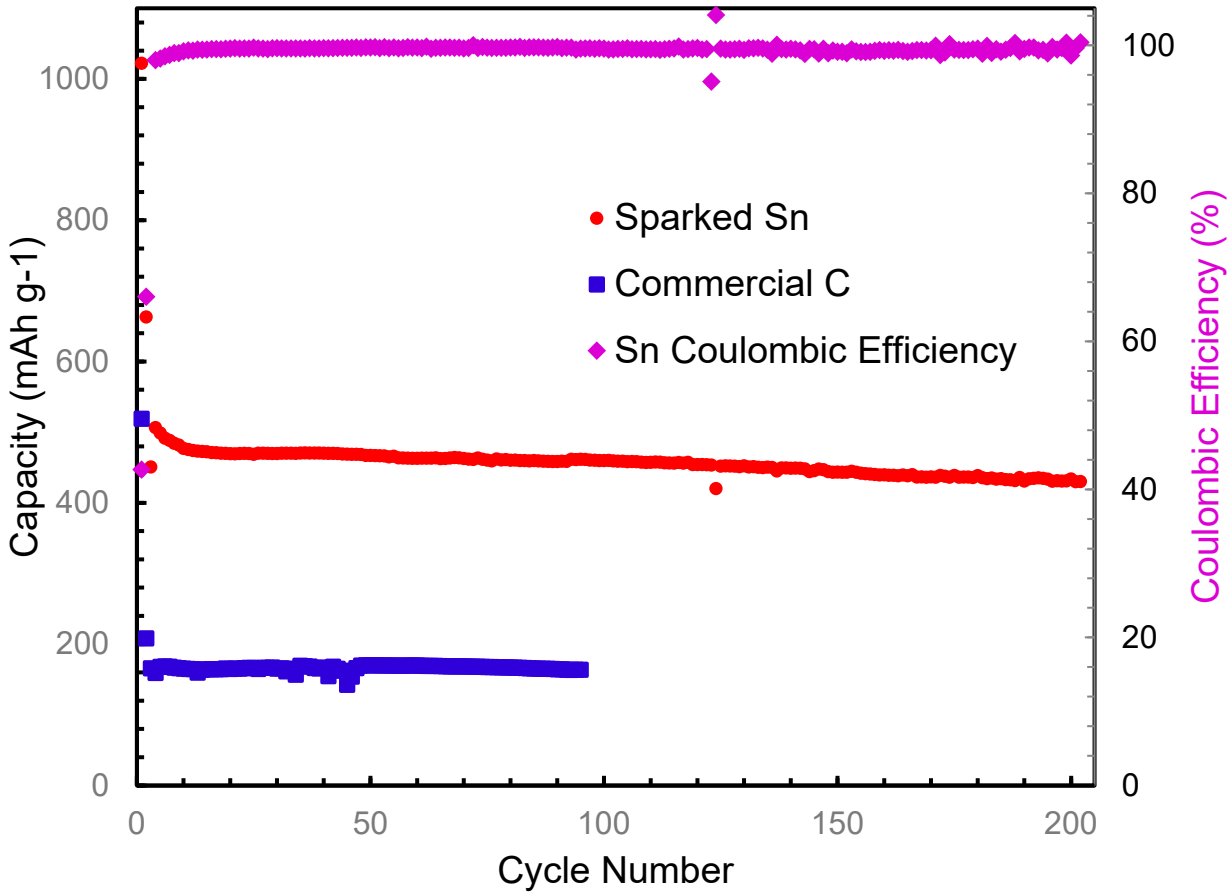

Figure 4. Capacity and coulombic efficiency of SPE (Sparked) Sn nanoparticles (10:70:5:15 electrode) and a commercial graphite electrode (80:5:15). The commercial graphite was only tested for 100 cycles.

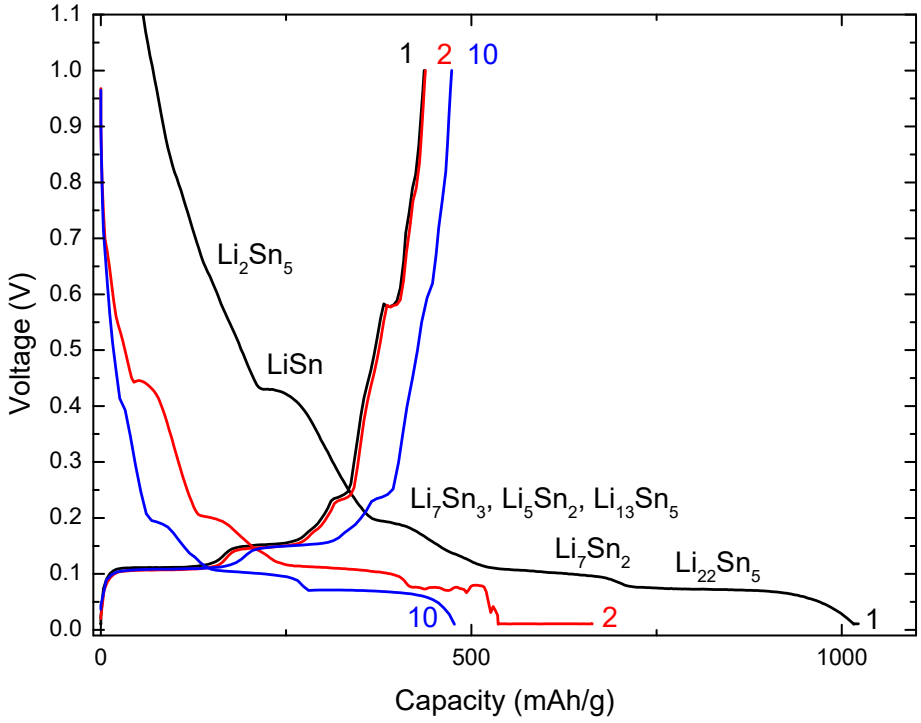

Figure 5. Potential difference vs. capacity for the 1st, 2nd and 10th cycles of the SPE Sn nanoparticles. Plateaus are labeled for the various Li_xSn_y phases.

The outstanding cycling stability of the 10 wt.% SPE Sn electrode is shown by the coulombic efficiency approaching 100% within 10 cycles. The exceptionally stable high-capacity performance is attributed to two main features of the nanoparticles: the carbon coating and the nanometric size. The carbon coating, though likely reducing the conductivity of the particles, provides a protective layer to prevent oxidation, prevent agglomeration, maintain contact within the electrode, and minimize volume expansion [7,8]. Additionally, the XPS results and the reversible capacity indicate the stronger chemical connection between carbon and metallic Sn in these SPE Sn nanoparticles, which is usually weak and results in capacity fade, especially in composite materials [7]. The majority of the Sn particles are below the 200 nm critical size for Sn for fracture as predicted by Huggins and Nix, even without taking into account unique nano-mechanics [22], so the anode structure can be maintained through extensive charge/discharge cycling [8]. Therefore, these novel carbon-coated Sn nanoparticles produced using spark plasma erosion are able to overcome the last two obstacles of commercial Sn anodes: poor cycling stability and low coulombic efficiency [8].

With only a 10 wt.% addition of these one-step SPE Sn particles, the current commercial total cell capacity could increase from ~62 mAh/g to ~70 mAh/g. This is an incredible ~10% increase in the overall capacity of the lithium-ion cell for such a small addition [23]. For the current method of electrode processing and cell assembly, these novel SPE nanoparticles are drop-in ready for lithium-ion battery manufacturing as this production method is immediately scalable to the commercial level, solving another key issue of Sn anode nanomaterials [9]. Additionally, it is expected that these carbon-coated Sn nanoparticles will have a high-rate capability due to their high conductivity and nanoscale size, which is one of the primary driving forces for investigating Sn as an anode material [7].

A significant benefit of this approach is the capacity improvement that is obtained with only 10 wt.% of the higher-cost Sn nanoparticles (versus graphite) combined with a commercially available graphite for the anode. This means a cell capacity increase without a large increase in cost. Most of the higher-capacity nanostructured Sn anodes require ~80 wt.% or more of higher-cost active material within the anode, and most of these materials are complex to produce, which means they would have an even higher cost than the novel SPE Sn nanoparticles in this work. Even recently developed 'facile' methods, such as electrospray-carbonization to produce a Sn/SnO_2/nitrogen-doped superstructure, require more costly precursors, such as SnO_2 nanoparticles and polyacrylonitrile solution with multiple processing steps [24,25]. Another 'simple' strategy for controlled synthesis of mesoporous carbon containing Sn/SnO and SnO_2 nanoparticles carbonized disodium stannous citrate, which still requires a complicated chemical precursor [26]. Still, other methods such as co-precipitation to produce hierarchical Sn^{4+}-doped $TiNb_2O_7$ nanospheres [27] or hierarchical microporous Si/Sn composites from etching melt-spun ribbons [28] are multistep procedures, utilize 60–70wt.% active material, and do not achieve the reversible ~460 mAh/g shown here [8]. So, while some methods may have achieved slightly higher capacities, such as ~640 mAh/g [24], ~670 mAh/g [26], ~600 mAh/g [29], or 550–710 mAh/g [9], truly simplified production combined with lower cost and a higher stable capacity has only truly been demonstrated by the novel SPE Sn nanoparticles in this study [15]. With further optimization, such as additional particle size control [30,31], carbon or oxide species optimization [32], and/or electrolyte/binder development [33], these SPE carbon-coated Sn nanoparticles have outstanding potential as a future anode material for next-generation Li-ion batteries.

4. Conclusions

Spark plasma erosion is a successful one-step method to produce carbon-coated Sn particles in the nanometer range. As an automated electro-mechanical method, spark plasma erosion shows great promise for the production of anode materials for lithium-ion batteries. The as-produced novel carbon-coated Sn nanoparticles show excellent high capacity (~460 mAh/g) and stable half-cell electrochemical performance with greater than

99.5% coulombic efficiency for 200 cycles, with only a 10 wt.% addition to commercial graphite. The SPE carbon-coated Sn nanoparticles are drop-in ready for present lithium-ion anode processing and would provide a ~10% increase in the total capacity of current commercial lithium-ion cells.

Author Contributions: Conceptualization, E.M.H.W., S.W.M. and I.E.A.; data curation, E.M.H.W. and L.M.R.; formal analysis, E.M.H.W.; funding acquisition, E.M.H.W., S.W.M. and I.E.A.; investigation, E.M.H.W. and L.M.R.; methodology, E.M.H.W., L.M.R., S.W.M. and I.E.A.; project administration, S.W.M. and I.E.A.; resources, E.M.H.W., S.W.M. and I.E.A.; supervision, S.W.M. and I.E.A.; validation, E.M.H.W.; visualization, E.M.H.W.; writing—original draft, E.M.H.W.; writing—review and editing, E.M.H.W., L.M.R., S.W.M. and I.E.A. All authors have read and agreed to the published version of the manuscript.

Funding: EMHW was supported by the NASA Aeronautics Scholarship Program and the NSF GK-12 Symbi program at ISU. Spark plasma erosion processing research, supervised by IEA, was supported by the Ames Lab Seed Fund and by the DOE, Office of Basic Energy Sciences, Division of Materials Sciences and Engineering. Ames National Laboratory is operated for the U.S. DOE by Iowa State University under Contract DE-AC02-07CH11358. The half-cell testing, supervised by SWM, was supported by the NSF [grant numbers DMR 0710564 and DMR 1304977] and the DOE, Sandia National Laboratory, and Arizona State University through contract number 11080469.

Data Availability Statement: The original contributions presented in this study are included in the article; further inquiries can be directed to the corresponding author.

Acknowledgments: The authors thank Jim Anderegg at Ames Laboratory for XPS examination of the nanoparticles and Rick Baldwin and James Wu at the NASA Glenn Research Center for helpful discussions.

Conflicts of Interest: The authors declare no conflict of interest.

References

1. Tarascon, J.M.; Armand, M. Issues and challenges facing rechargeable lithium batteries. *Nature* **2001**, *414*, 359–367. [CrossRef] [PubMed]
2. Winter, M.; Besenhard, J.O. Electrochemical lithiation of tin and tin-based intermetallics and composites. *Electrochim. Acta* **1999**, *45*, 31–50. [CrossRef]
3. Elia, G.A.; Panero, S.; Savoini, A.; Scrosati, B.; Hassoun, J. Mechanically milled, nanostructured Sn-C composite anode for lithium ion battery. *Electrochim. Acta* **2013**, *90*, 690–694. [CrossRef]
4. Xu, Y.; Liu, Q.; Zhu, Y.; Liu, Y.; Langrock, A.; Zachariah, M.R.; Wang, C. Uniform nano-Sn/C composite anodes for lithium ion batteries. *Nano Lett.* **2013**, *13*, 470–474. [CrossRef]
5. Lee, K.T.; Cho, J. Roles of nanosize in lithium reactive nanomaterials for lithium ion batteries. *Nano Today* **2011**, *6*, 28–41. [CrossRef]
6. Zhou, X.; Zou, Y.; Yang, J. Carbon supported tin-based nanocomposites as anodes for Li-ion batteries. *J. Solid State Chem.* **2013**, *198*, 231–237. [CrossRef]
7. Wu, C.; Zhu, G.; Wang, Q.; Wu, M.; Zhang, H. Sn-based nanomaterials: From composition and structural design to their electrochemical performances for Li- and Na-ion batteries. *Energy Storage Mater.* **2021**, *43*, 430–462. [CrossRef]
8. Ying, H.; Han, W.-Q. Metallic Sn-based anode materials: Application in high-performance lithium-ion and sodium-ion batteries. *Adv. Sci.* **2017**, *4*, 1700298. [CrossRef]
9. Li, W.; Sun, X.; Yu, Y. Si-, Ge-, Sn-based anode materials for lithium-ion batteries: From structure design to electrochemical performance. *Small Methods* **2017**, *1*, 1600037. [CrossRef]
10. Carrey, J.; Radousky, H.B.; Berkowitz, A.E. Spark-eroded particles: Influence of processing parameters. *J. Appl. Phys.* **2004**, *95*, 823–829. [CrossRef]
11. Berkowitz, A.E.; Harper, H.; Smith, D.J.; Hu, H.; Jiang, Q.; Solomon, V.C.; Radousky, H.B. Hollow metallic microspheres produced by spark erosion. *Appl. Phys. Lett.* **2004**, *85*, 940–942. [CrossRef]
12. Berkowitz, A.E.; Walter, J.L. Amorphous particles produced by spark erosion. *Mater. Sci. Eng.* **1982**, *55*, 275–287. [CrossRef]
13. Berkowitz, A.E.; Walter, J.L.; Wall, K.F. Magnetic properties of amorphous particles produced by spark erosion. *Phys. Rev. Lett.* **1981**, *46*, 1484–1487. [CrossRef]
14. Berkowitz, A.E.; Walter, J.L. Spark erosion: A method for producing rapidly quenched fine powders. *J. Mater. Res.* **1987**, *2*, 277–288. [CrossRef]
15. White, E.M.H. Development of Spark Plasma Erosion to Enable Scalable Direct Synthesis of High Performance Nano-Particulate Materials for Energy Storage Applications. Doctoral Dissertation, Iowa State University, Ames, IA, USA, 2014.

16. Beattie, S.D.; Larcher, D.; Morcrette, M.; Simon, B.; Tarascon, J.-M. Si electrodes for Li-ion batteries—A new way to look at an old problem. *J. Electrochem. Soc.* **2008**, *155*, A158–A163. [CrossRef]
17. White, E.M.H.; Rueschhoff, L.M.; Kobayashi, T.; Bloh, J.Z.; Martin, S.W.; Anderson, I.E. One-Step Spark Plasma Erosion Processing of Carbon-Coated Sn-Si Nanoparticles for Lithium-Ion Battery Anodes. *Surfaces* **2024**, *7*, 725–738. [CrossRef]
18. Wang, Y.; Zhang, T.; Xiao, J.; Tian, X.; Yuan, S. Enhancing electrochemical performance of ultrasmall Fe_2O_3-embedded carbon nanotubes via combusting-induced high-valence dopants. *J. Mater. Sci. Technol.* **2023**, *134*, 142–150. [CrossRef]
19. Norton, P.R. An investigation of the adsorption of oxygen and oxygen containing species on platinum by photoelectron spectroscopy. *Surf. Sci.* **1975**, *47*, 98–114. [CrossRef]
20. Wen, C.J.; Huggins, R.A. Thermodynamic study of the lithium-tin system. *J. Electrochem. Soc.* **1981**, *128*, 1181–1187. [CrossRef]
21. Wang, B.; Luo, B.; Li, X.; Zhi, L. The dimensionality of Sn anodes in Li-ion batteries. *Mater. Today* **2012**, *15*, 544–552. [CrossRef]
22. Huggins, R.A.; Nix, W.D. Decrepitation model for capacity loss during cycling of alloys in rechargeable electrochemical systems. *Ionics* **2000**, *6*, 57–63. [CrossRef]
23. Kasavajjula, U.; Wang, C.; Appleby, A.J. Nano- and bulk-silicon-based insertion anodes for lithium-ion secondary cells. *J. Power Sources* **2007**, *163*, 1003–1039. [CrossRef]
24. Shen, Z.; Guo, X.; Ding, H.; Yu, D.; Chen, Y.; Li, N.; Zhou, H.; Zhang, S.; Wu, J.; Pang, H. Construction of ternary Sn/SnO_2/nitrogen-doped carbon superstructures as anodes for advanced lithium-ion batteries. *NanoResearch* **2024**. [CrossRef]
25. Xu, Y.; Zhu, Y.; Liu, Y.; Wang, C. Electrochemical performance of porous carbon/tin composite anodes for sodium-ion and lithium-ion batteries. *Adv. Energy Mater.* **2013**, *3*, 128–133. [CrossRef]
26. Liu, K.; Guo, D.; Zhao, D.; Zhao, P.; Ma, R.; Geng, F.; Zhang, Q.; Zhang, S.; Song, Y.; Sun, J. A simple strategy for the controllable synthesis of tin-based anode materials and their lithium storage performances. *J. Energy Storage* **2024**, *100*, 113600. [CrossRef]
27. Wang, X.; Xu, Z.; Amzil, S.; Cheng, Y.-J.; Lin, L.; Ji, Q.; Liang, S.; Zhu, J.; Duan, J.; Zheng, T.; et al. Fast, one-step in situ synthesis of a hierarchical Sn^{4+}-doped $TiNb_2O_7$ nanosphere as a high-performance anode material. *ChemistrySelect* **2024**, *9*, e202402449. [CrossRef]
28. Hao, Q.; Hou, J.; Ye, J.; Yang, H.; Du, J.; Xu, C. Hierarchical microporous Si/Sn composite: Easy preparation and optimized performances towards lithium storage. *Electrochim. Acta* **2019**, *306*, 427–436. [CrossRef]
29. Jin, Z.; Ben, L.; Yu, H.; Zhao, W.; Zhao, W.; Huang, X. A facile method to synthesize 3D structured Sn anode material with excellent electrochemical performance for lithium-ion batteries. *Prog. Nat. Sci. Mater. Int.* **2020**, *30*, 456–460. [CrossRef]
30. Gonzalez, J.; Sun, K.; Huang, M.; Dillon, S.; Chasiotis, I.; Lambros, J. X-ray microtomography characterization of Sn particle evolution during lithiation/delithiation in lithium ion batteries. *J. Power Sources* **2015**, *285*, 205–209. [CrossRef]
31. Zhang, T.; Fu, L.J.; Gao, J.; Wu, Y.P.; Holze, R.; Wu, H.Q. Nanosized tin anode prepared by laser-induced vapor deposition for lithium ion battery. *J. Power Sources* **2007**, *174*, 770–773. [CrossRef]
32. Wang, J.; Kober, D.; Shao, G.; Epping, J.D.; Görke, O.; Li, S.; Gurlo, A.; Bekheet, M.F. Stable anodes for lithium-ion batteries based on tin-containing silicon oxycarbonitride ceramic nanocomposites. *Mater. Today Energy* **2022**, *26*, 100989. [CrossRef]
33. Tu, S.; Ai, X.; Wang, X.; Gui, S.; Cai, Z.; Zhan, R.; Tan, Y.; Liu, W.; Yang, H.; Li, C.; et al. Circumventing chemo-mechanical failure of Sn foil battery anode by grain refinement and elaborate porosity design. *J. Energy Chem.* **2021**, *62*, 477–484. [CrossRef]